PRODUCTION PROCESSES OF BOULDERS AND REGOLITH ON LUNAR CRATER SLOPES INFERRED FROM TOPOGRAPHIC FEATURE AND ROCK ABUNDANCE. A. Ikeda[1], H. Kumagai[1], and T. Morota[2], [1]Graduate School of Environmental Sciences, Nagoya University, Nagoya, Japan (ikeda.ayame.z6@s.mail.nagoya-u.ac.jp), [2]Graduate School of Science, The University of Tokyo, Tokyo, Japan.

Introduction: There is a wide variety of surface condition among celestial bodies. On sub-kilometer-sized asteroids such as Ryugu, Itokawa, and Bennu, there are many boulders [e.g., 1], while the Moon is widely covered by fine regolith [2]. Movements of boulders and regolith were also found on these bodies [1,3]. It has been considered that impacts and thermal fatigue may produce boulders and regolith on celestial surfaces. Thermal fatigue induced by solar heating is a mechanism for in-place rock breakdown capable of generating fine-scaled regolith layers [4]. Cambioni et al. [5] suggested that fine regolith formation is mainly controlled by thermal fatigue on asteroids consisting of porous rocks. They also noted that low-porosity rocks produce more fine regolith than high-porosity rocks by thermal fatigue.

On the Moon, high resolution images taken by Lunar Reconnaissance Orbiter (LRO) and Kaguya identified boulders densely distributed on crater walls (boulder sources) and boulders fallen down slopes [e.g., 3,6,7]. However, detailed boulder and regolith formation processes remain unknown. To investigate these processes on inner walls of lunar craters, we analyzed densities of small craters, distributions of boulder sources and rock abundance, and slope profiles using high resolution images gained by LRO and Kaguya.

Data and Methods: We counted the density of small craters ($D \geqq 5$ m) using LRO Narrow Angle Camera data, and calculated slope angles from digital terrain model (DTM) data created from stereo images taken by Terrain Camera onboarded Kaguya. We also constructed topographic slope profiles of the inner walls from DTM and compared them to the topographic profiles calculated from the one-dimensional diffusion model with a space-varying diffusion coefficient (κ). We used the rock abundance (RA) map derived from LRO Diviner observation [8,9]. This map represents the areal fraction of the surface covered by rock fragments roughly > 1 m [8–10]. We compared the RA density, which is defined by RA values accumulated within the target region and divided by the area, with the crater retention age in the region.

We investigated the following four crater slopes: southern slope in the Schrödinger basin (79.35°–79.48°S, 128.4°–129.5°E); an 8-kilometer-sized crater in southern Lorentz basin (28.5°–29°N, 262.5°–263°E); Milne N crater (35.25°–36.4°S, 110.7°–111.9°E); and the southern slope of Hilbert W crater (17.0°–17.65°S, 107.3°–108.3°E).

Results and Discussion: We analyzed the distributions of boulder sources and small craters, and found that boulder sources were on upslope areas. The crater retention ages estimated from the densities of small craters in these regions were 1–20 Ma. These young ages suggest that regolith flow has erased small craters on the slopes. We found that areas with high

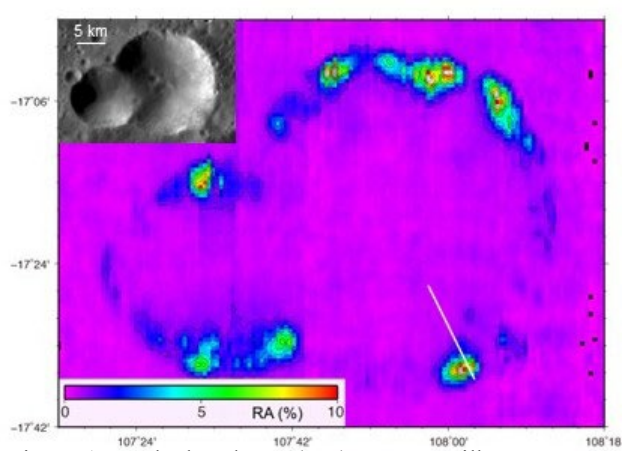

Figure 1. Rock abundance (RA) map on Hilbert W crater. The white line represents the section shown in Figure 2. The inset shows a panchromatic image of the crater (https://quickmap.lroc.asu.edu/).

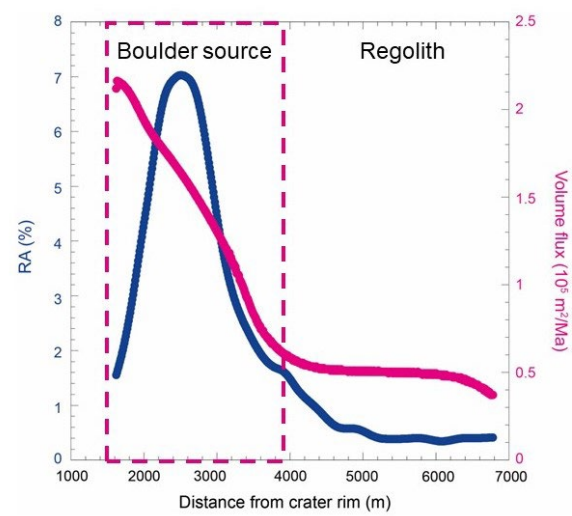

Figure 2. Rock abundance (RA) values and volume flux per unit length on the slope of Hilbert W crater.

RA values correspond to boulder sources on the upslope areas on all the crater slopes (Figure 1).

Our estimates show that the RA density tends to decrease with increasing crater retention age, indicating that the slopes with higher RA values tend to be young.

We also found that the topographic profile of the SE inner wall of Hilbert W crater is characterized by bulge and depression. The depression occurred below boulder sources and the bulge was beneath the depression. Fassett and Thomson [11] characterized the degradation of craters (smaller than 5 km in diameter) by using a topographic diffusion model assuming a constant diffusion coefficient in each crater, and estimated the crater degradation state (κt, t is time) to be about 10^3 to 2.5×10^4 m^2 corresponding to κ of 2–20 m^2/Ma. We found that the topographic feature on the Hilbert W crater slope cannot be reproduced by using a constant κ value, but by increasing κt toward the crater rim. If the topographic feature was formed during about 1 Ma, κ was estimated to be 1×10^5–6×10^5 m^2/Ma, which is about 10^4 times larger than the previous estimate. Assuming that the topographic feature was formed by regolith diffusive movement, we calculated volume flux of regolith using the estimated diffusion coefficient and topography (h) through the following equation:

$$q = \kappa\,|\nabla h|,$$

where q is volume flux per unit length (m^2/Ma). Our calculations indicated that areas with large q values correspond to boulder sources with high RA values (Figure 2). This result suggests that regolith is produced more efficiently in the boulder sources and regolith movement degrades the crater slope rapidly. Our finding of a negative correlation between the RA density and crater retention age implies that such rapid crater degradation is controlled by the distributions of boulder sources on crater slopes.

Conclusion: We estimated the distributions of boulder sources, small craters, and RA values in four crater slopes and reproduced the topographic feature in Hilbert W crater using the topographic diffusion model with a space-varying diffusion coefficient. We found that areas with high RA values correspond to boulder sources, and large volume flux was estimated in boulder sources. Our results suggest that regolith is efficiently produced by thermal fatigue in boulder sources and resultant regolith movement rapidly degrades crater slopes.

Acknowledgement: This study was supported by JSPS Grand-in-Aide 20H00194 and "Nagoya University Interdisciplinary Frontier Fellowship" Grant Number JPMJFS2120 supported by Nagoya University and JST.

References: [1] Sugita, S. et al. (2019) *Science*, *364*, eaaw0422. [2] Shoemaker, E. M. et al. (1969) *JGR*, *74*, 6081–6119. [3] Bickel, V. T. et al. (2021) *JGR: Planets*, *126*, e2021JE006824. [4] Delbo, M. et al. (2014) *Nature 508*, 233–236. [5] Cambioni, S. et al. (2021) *Nature 598*, 49–52. [6] Kumar, P. S. et al. (2016) *JGR: Planets*, *121,* 147–179. [7] Ikeda, A. et al. (2022) *JGR: Planets*, *127*, e2021JE007176 [8] Paige et al. (2011) LRO-L-DLRE-5-GDR-V1.0 [dataset] [9] Bandfield, J. L. et al (2011) *JGR*, *116*, E00H02, [10] Vanga, S. et al. (2022) *GRL*, *49*, e2021GL096710. [11] Fassett, C. I. and Thomson, B. J. (2014) *JGR: Planets*, *119*, 2255–2271.